Received: 1 September 2018 | Revised: 2 February 2019 | Accepted: 24 February 2019

DOI: 10.1002/nbm.4097

RESEARCH ARTICLE

WILEY NMR IN BIOMEDICINE

Magnetization transfer in liposome and proteoliposome samples that mimic the protein and lipid composition of myelin

Weiqi Yang[1] | Jae-Seung Lee[1,2] | Maureen Leninger[1] | Johannes Windschuh[2] | Nathaniel J. Traaseth[1] | Alexej Jerschow[1]

[1] Department of Chemistry, New York University, New York, NY, USA

[2] Department of Radiology, New York University Langone Medical Center, New York, NY, USA

Correspondence
Alexej Jerschow, Department of Chemistry, New York University, New York, NY, USA.
Email: alexej.jerschow@nyu.edu

Funding information
US National Science Foundation, Grant/Award Number: CHE 1710046; National Institutes of Health, Grant/Award Numbers: R01AI108889 and R01EB016045

Although magnetization transfer (MT) has been widely used in brain MRI, for example in brain inflammation and multiple sclerosis, the detailed molecular origin of MT effects and the role that proteins play in MT remain unclear. In this work, a proteoliposome model system was used to mimic the myelin environment and to examine the roles of protein, cholesterol, brain cerebrosides, and sphingomyelin embedded in the liposome matrix. Exchange parameters were determined using a double-quantum filter experiment. The goal was to determine the relative contributions to exchange and MT of cerebrosides, sphingomyelin, cholesterol, and proteins in 1,2-dimyristoyl-*sn*-glycero-3-phosphocholine bilayers. The main finding was that cerebrosides produced the strongest exchange effects, and that these were even more pronounced than those found for proteins. Sphingomyelin (which also has exchangeable groups at the head of the fatty acid chains, albeit closer to the lipid acyl chains) and cholesterol showed only minimal transfer. Overall, the extracted exchange rates appeared much smaller than commonly assumed for -OH and -NH groups.

KEYWORDS

chemical exchange saturation transfer, magnetization transfer, white matter diseases

1 | INTRODUCTION

Magnetization transfer (MT) has become a powerful and popular technique for imparting image contrast based on chemical exchange or cross-relaxation in macromolecular assemblies, especially for use in brain MRI. This contrast has been shown to produce indicators for certain abnormalities, including brain inflammation and multiple sclerosis.[1-4] In MT, the longitudinal magnetization of rigid or semisolid-like tissue is partially saturated and transferred to the free water pool. Residual dipolar couplings are responsible for the communication of the saturation levels towards the exchange site, which in turn transmits the saturation to water. There are two generally accepted mechanisms for the transmission of saturation levels to the water pool: (a) chemical exchange and (b) cross-relaxation through the relayed nuclear Overhauser effect (NOE), with the latter often being very weak or non-existent.[5-7] MT contrast allows quantification of the macromolecular pool fraction to a certain extent, and such quantities have been correlated with myelin content as well as water content change in myelin tissue.[4,8,9]

Myelin is a multilayered stack of membranes consisting of 80% lipids by dry weight. The wrapping of multiple layers of myelin membrane sheets around an axon is of fundamental importance for the function of the nervous system. The lipids within myelin are composed of glycosphingolipids (~27%), cholesterol (~43%), plasmalogens (~16%), and other phospholipids (sphingomyelin, phosphatidylinositol,

Abbreviations used: DDM, *n*-dodecyl β-D-maltoside; DMPC, 1,2-dimyristoyl-*sn*-glycero-3-phosphocholine; DQ, double quantum; DQF, double-quantum filter; MBP, myelin basic protein; MT, magnetization transfer; NOE, nuclear Overhauser effect; PLP, proteolipid protein; ZQ, zero quantum.

phosphatidylserine, etc).[10,11] The protein-to-lipid ratio by weight is lower in myelin (~0.25) compared with a plasma membrane (from 1 to 4). There are generally two types of protein in the myelin structure: the proteolipid protein (PLP) and myelin basic protein (MBP). PLP is a transmembrane protein that plays a role in the adhesion of the extracellular leaflets of the myelin membrane. MBP is a peripheral membrane protein that helps bring myelin bilayers close together by a combination of electrostatic and hydrophobic forces.[10] It has been demonstrated that one can directly image the short T_2 signal component in myelin using ultra-short TE imaging methods.[11] For human in vivo applications, such short echo times are typically unattainable. MT contrast provides an alternative, which, through repeated chemical exchange, leads to contrast enhancement for the detection of myelin. The mechanism of MT is of interest, because it may be relevant for the interpretation of imaging results and may allow the extraction of specific information on myelin composition and its environment.

Previous work examined the detailed molecular origin of MT contrast. Fralix et al suggested that cholesterol was a key component for the generation of MT in lipid systems.[12] Kucharczyk et al examined MT in synthetic lipids and concluded that galactocerebroside components had the largest contribution to MT.[13] Malyarenko et al and Lee et al identified that exchangeable groups were essential for effective MT, through experiments with a liquid crystal system,[14,15] thus direct NOE from macromolecules to water could be ruled out as the primary contrast mechanisms.[16,17] The quantitative MT and the super-Lorentzian model were also used to detect the abnormality in human brains,[2,18-20] but MT research on multilamellar lipid phases was limited. The contribution of cholesterol and protein concentration to the modulation of the MT effect remains unclear to date. Here, we investigate the detailed molecular origin of MT effects by using a liposome and proteoliposome model system containing 1,2-dimyristoyl-*sn*-glycero-3-phosphocholine (DMPC) and a 44 kDa membrane protein with transmembrane and extra-membrane portions to mimic the white matter system.[13,21] The liposome model system used here had multilamellar phases, which display orientational averaging —similar to what one would find in the brain in voxels where a distribution of orientations is present. The protein system we chose (fusion of EmrE[22], and maltose binding protein) bears a strong resemblance to MBP, in terms of both the size of the soluble protein and the number of transmembrane domains of the membrane spanning region of MBP. We also examined the roles of cholesterol, brain cerebrosides, and sphingomyelin embedded in the liposome due to their large amounts of myelin and relatively large numbers of labile protons.[11] A double-quantum filter (DQF) experiment[17] is shown to be particularly useful for extracting transfer parameters. Although myelin tissue is more complex than the samples considered here, we aimed to reduce the complexity and confine the study to the investigation of the differential effects between different components within liposomes. The results may be valuable for the ultimate understanding of MT processes in myelin tissue.

2 | THEORETICAL BACKGROUND

A *z*-spectrum is commonly used to study the MT effect for a certain spin system.[15,21,23,24] It represents the collection of the water signals after presaturation at different frequency offsets, normalized to the signal without any presaturation.[25] This approach has certain limitations. For example, in a *z*-spectrum it is very difficult to separate the exchange rates from the pool sizes in such measurements, especially in the presence of a sizable macromolecular signal.[26] In this study, we hence chose another approach to tag the macromolecular pool using a DQF-MT experiment.[17] Upon selecting the semisolid signal, one can follow the buildup of magnetization in the water pool resulting from the exchange with the macromolecular pool with this sequence.

This DQF-MT sequence was previously established as a method to examine exchange processes in a collagen-water system.[17] The differentiation between the pools is achieved by the generation of double-quantum (DQ) coherences in the macromolecular pool due to residual dipolar couplings. Following an exchange period, one can track the dynamics of the exchange process originating from the macromolecules.[17] In this way, it was possible to separate the macromolecular magnetization from the one of from bulk water and therefore monitor its MT process.

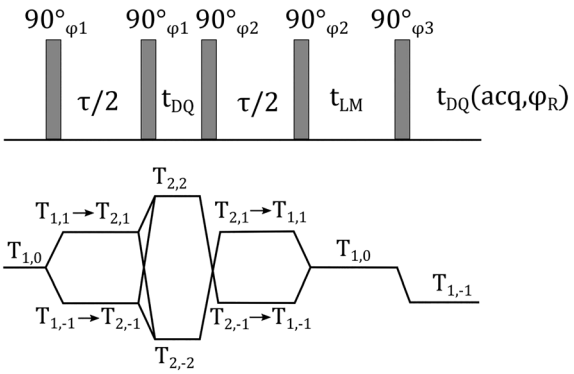

FIGURE 1 DQF-MT pulse sequence. 16-step phase cycling was used: φ_1 = (0, 90°, 180°, 270°, 90°, 180°, 270°, 0, 180°, 270°, 0, 90°, 270°, 0, 90°, 180°), φ_2 = (0, 0, 0, 0, 90°, 90°, 90°, 90°, 180°, 180°, 180°, 180°, 270°, 270°, 270°, 270°, φ_3 = 0, φ_R = (180°, 0)

The DQF-MT sequence used in this study is shown in Figure 1. Key functions of the sequence[17] are described here for convenience. Following the initial 90° pulse, second rank tensors $T_{2,\pm1}$ are generated during the first $\tau/2$ period. The second 90° pulse converts these to DQ coherence, which is selectively filtered by a phase cycle. The third 90° pulse converts the filtered tensors $T_{2,\pm2}$ to $T_{2,\pm1}$, which evolve into $T_{1,\pm1}$ during the second $\tau/2$ period. After the fourth 90° pulse, the zero-quantum (ZQ) coherence $T_{1,0}$ is selectively filtered by a phase cycle and a subsequent waiting period t_{LM} allows for exchange. Following this exchange period, the last 90° pulse excites single-quantum coherence for detection.

The combination of the DQ and ZQ filters is implemented by a 16-step phase cycle, φ_1 = (0°, 90°, 180°, 270°, 90°, 180°, 270°, 0°, 180°, 270°, 0°, 90°, 270°, 0°, 90°, 180°), φ_2 = (0°, 0°, 0°, 0°, 90°, 90°, 90°, 90°, 180°, 180°, 180°, 180°, 270°, 270°, 270°, 270°, φ_3 = 0°, φ_R = (180°, 0°), instead of the 64-step phase cycle presented in Reference 17. We tested both phase cycling schemes and chose the former because it performed better in terms of filtering out the free water signal and saving experiment time. The first two RF pulses were grouped to select DQ coherences. The third and fourth RF pulses were grouped to select ZQ coherences.

During the exchange period t_{LM}, the evolution of the ZQ coherences may be described using chemical exchange and cross-relaxation models.[17,27,28] The heterogeneous biological system can be treated as a two-phase proton system. Water and liposome protons constitute the two phases, and they are denoted by subscripts w and l, respectively. A common spin temperature will be rapidly established within the liposome and water phases by spin diffusion and MT and by rapid chemical exchange between different environments, respectively.[27,28] This assumption can be justified on the basis of the relative sizes of the dipolar couplings along the lipid chain. It was shown that the following equations could describe the exchange process during the period t_{LM}[17,28]:

$$M_{zl} = m_{zl}(t_{LM}=0)\left(a_+ e^{-t_{LM}/T_{1+}} + a_- e^{-t_{LM}/T_{1-}}\right) + m_{zw}(t_{LM}=0)b\left(e^{-t_{LM}/T_{1-}} - e^{-t_{LM}/T_{1+}}\right) \quad (1)$$

$$M_{zw} = m_{zl}(t_{LM}=0)\frac{p_w}{p_l}b\left(e^{-t_{LM}/T_{1-}} - e^{-t_{LM}/T_{1+}}\right) + m_{zw}(t_{LM}=0)\left(a_- e^{-t_{LM}/T_{1+}} + a_+ e^{-t_{LM}/T_{1-}}\right)$$

$$a_\pm = \frac{1}{2}\left[1 \pm \frac{R_{1l} - R_{1w} + k - 2p_l k}{\sqrt{(R_{1l}-R_{1w}+k)^2 - 4p_l k(R_{1l}-R_{1w})}}\right]$$

$$b = \frac{p_l k}{\sqrt{(R_{1l}-R_{1w}+k)^2 - 4p_l k(R_{1l}-R_{1w})}}$$

$$\frac{1}{T_{1\pm}} = \frac{1}{2}\left[R_{1l} + R_{1w} + k \pm \sqrt{(R_{1l}+R_{1w}+k)^2 - 4p_l k(R_{1l}-R_{1w})}\right].$$

Here $m_{zl}(t_{LM}=0)$ and $m_{zw}(t_{LM}=0)$ are the longitudinal magnetizations M_{zl} and M_{zw} for liposomes and water at $t_{LM}=0$, respectively. R_{1l} and R_{1w} are the longitudinal relaxation rates for liposomes and water. p_l and p_w represent the fractions of the protons involved in the exchange process residing on the liposomes and water. The exchange rate, k, is the sum of the forward and backward reactions rates. When t_{LM} is zero or close to zero, chemical exchange has not developed yet, and we can assume $m_{zw}(t_{LM}=0)=0$. For a normalized signal strength, we can assume $m_{zl}(t_{LM}=0)=1$. Equation (1) then becomes

$$M_{zl} = \left(a_+ e^{-t_{LM}/T_{1+}} + a_- e^{-t_{LM}/T_{1-}}\right) \quad (2)$$

$$M_{zw} = \frac{p_w}{p_l}b\left(e^{-t_{LM}/T_{1-}} - e^{-t_{LM}/T_{1+}}\right)$$

$$a_\pm = \frac{1}{2}\left[1 \pm \frac{R_{1l} - R_{1w} + k - 2p_l k}{\sqrt{(R_{1l}-R_{1w}+k)^2 - 4p_l k(R_{1l}-R_{1w})}}\right]$$

$$b = \frac{p_l k}{\sqrt{(R_{1l}-R_{1w}+k)^2 - 4p_l k(R_{1l}-R_{1w})}}$$

$$\frac{1}{T_{1\pm}} = \frac{1}{2}\left[R_{1l} + R_{1w} + k \pm \sqrt{(R_{1l}+R_{1w}+k)^2 - 4p_l k(R_{1l}-R_{1w})}\right].$$

The exchange process between the lipids and water was dominated by the exchange rate k, the longitudinal relaxation rate for lipids and water, and the proton ratio between the fractions of the protons involved in the MT process.

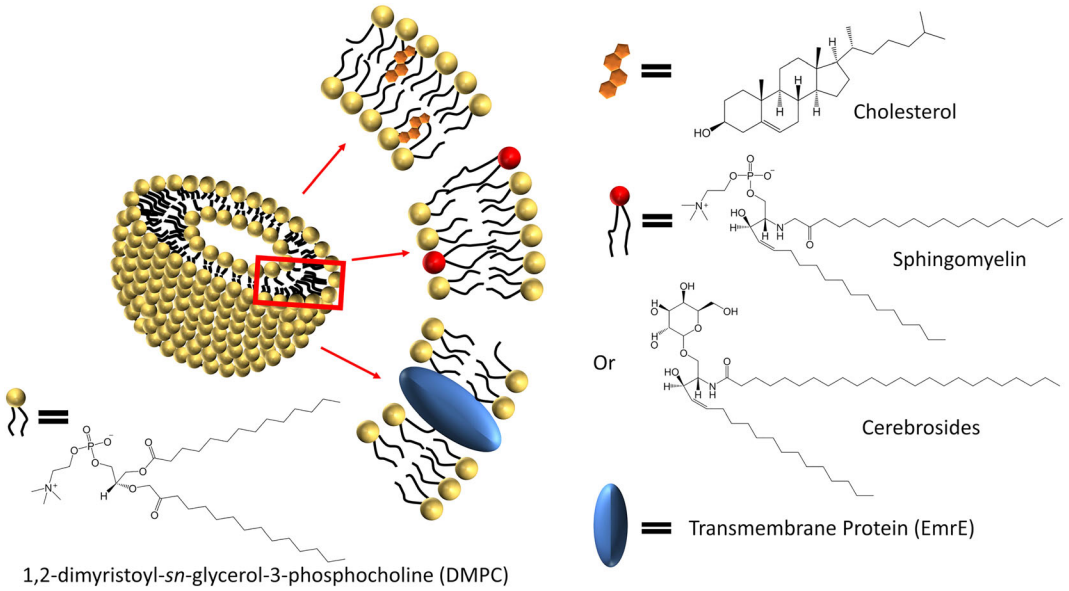

FIGURE 2 Schematic diagram of liposomes used for measurements of MT in a system designed to mimic white matter. The primary component of the liposomes was DMPC. Four additional components were included with the goal of delineating the MT mechanisms: Cholesterol, sphingomyelin, cerebrosides, and a fusion protein consisting of maltose binding protein and EmrE. The chemical structures of sphingomyelin and cerebrosides were representative structures since a lipid extract would display a range of possible lipid lengths and saturation levels. Note that the samples were prepared in multilamellar phases

3 | MATERIALS AND METHODS

3.1 | Sample preparation

Figure 2 shows a schematic diagram of liposomes used for measurements of MT in a system designed to mimic the multilamellar phase structure in white matter. These also display similar orientational averaging. Please note that the samples could not truly mimic white matter because of the tissue's complexity. The primary component of the liposomes was DMPC. Four additional components were included with the goal of delineating the MT mechanisms: cholesterol, sphingomyelin, cerebrosides, and a fusion protein consisting of maltose binding protein and EmrE. The liposomes were prepared in multilamellar phases.

Liposome samples were prepared by dissolving DMPC (Avanti Polar Lipids, MW = 677.93 g/mol) in a 3:1 mixture of chloroform:methanol and dried under nitrogen gas to a thin film. To remove residual solvent, the film was dried overnight under vacuum.[29,30]

Sphingomyelin (extract from porcine brain, Avanti Polar Lipids, Alabaster, AL, USA, MW = 760.33 g/mol), cholesterol (Sigma-Aldrich, MW = 386.65 g/mol), or cerebrosides (extract from porcine brain; Avanti Polar Lipids, MW = 781.95 g/mol) were co-dissolved with DMPC at a 10% w/w concentration. The mixture was co-dissolved in a 3:1 mixture of chloroform:methanol, dried under nitrogen gas to a thin film, and dried overnight under vacuum.

The samples with protein contained a fusion construct with maltose binding protein adjoined to EmrE. Maltose binding protein (globular) was positioned at the N-terminal side of the fusion construct, while EmrE (transmembrane) was at the C-terminal end. To reconstitute the protein into liposomes, the thin film of DMPC was rehydrated in 100mM Na_2HPO_4 (pH = 7.0), 20mM NaCl, and *n*-dodecyl β-D-maltoside (DDM) solubilized fusion protein. Samples were incubated overnight with Bio-Beads (Bio-Rad, Hercules, CA, USA) to remove the detergent. The liposomes were pelleted at 300 000 *g* for 2 h at 8°C using a TLA-110 rotor (Beckman-Coulter, Brea, CA, USA).[29,30]

All samples were resuspended in 100mM Na_2HPO_4, 20mM NaCl at a pH of 7.0 and subjected to ten freeze/thaw cycles. The final composition was 300 μL buffer, 30 mg DMPC, and 3 mg of the respective additive (sphingomyelin, cholesterol, cerebrosides, or protein), as summarized in Table 1. The liposome suspensions were placed in a 5 mm o.d. NMR tube for subsequent spectroscopic measurements.

3.2 | NMR data acquisition

All experiments were performed on an Avance I spectrometer (Bruker, Billerica, MA, USA) operating at 400.13 MHz for ^{1}H. The duration of the 90° pulse was 5.3 μs. The longitudinal T_1 relaxation times were measured for liposome samples using the inversion recovery experiment with a

TABLE 1 The longitudinal relaxation time for water (w) and lipids (l) of each liposome sample measured using an inversion recovery experiment

Sample number:	1	2	3	4	5
Composition:	DMPC	DMPC + sphingomyelin	DMPC + cerebrosides	DMPC + cholesterol	DMPC + protein
R_{1w} (1/s)	0.46	0.48	0.52	0.41	0.43
R_{1l} (1/s)	7.14	6.25	7.14	2.13	1.72

recovery delay of 20 s. All the experiments were carried out at room temperature (19°C). Recovery delays for individual samples were adjusted to be five times the corresponding T_{1w} values shown in Table 1.

Z-spectra under single RF irradiations and DQF spectra were obtained from each liposome sample. The z-spectra were obtained with a 5 s long continuous wave presaturation pulse followed by a 90° readout pulse. The amplitude ($\gamma B_1/2\pi$) of the presaturation pulse was 500 Hz for all samples. Four transients were recorded for each frequency offset from −40 000 Hz to 40 000 Hz. The delay between each scan TR was five times the corresponding T_{1w} values as derived from Table 1. The RF frequency offsets for the z-spectrum measurement were (−120 000 Hz, −40 000 Hz, −36 000 Hz, −32 000 Hz, −28 000 Hz, −24 000 Hz, −22 000 Hz, −20 000 Hz, −18 000 Hz, −16 000 Hz, −14 000 Hz, −12 000 Hz, −10 000 Hz, −8000 Hz, −6000 Hz, −5000 Hz, −4000 Hz, −3000 Hz, −2000 Hz, −1000 Hz, −800 Hz, −400 Hz, −200 Hz, 0, 200 Hz, 400 Hz, 800 Hz, 1000 Hz, 2000 Hz, 3000 Hz, 4000 Hz, 5000 Hz, 6000 Hz, 8000 Hz, 10 000 Hz, 12 000 Hz, 14 000 Hz, 16 000 Hz, 18 000 Hz, 20 000 Hz, 22 000 Hz, 24 000 Hz, 28 000 Hz, 32 000 Hz, 36 000 Hz, 40 000 Hz, 120 000 Hz).

DQF spectra were obtained by the DQF-MT sequence given as a function of τ/2 with $t_{LM} = t_{DQ} = 2$ μs. The number of averages for each scan was 16, which corresponded to one complete phase cycle, as shown in in Figure 1. DQF spectra were obtained as a function of t_{LM} with τ/2 = 15 μs. The τ delay was first optimized by observing the maximum DQ excitation. The τ delays ranged from 2 to 180 μs. As seen in Figure S1, the broad lipid peak was strongest when τ/2 = 15 μs. As shown in Figures S2-S6, subsequent DQF experiments were performed with fixed τ/2 = 15 μs and variable 14 to 16 exchange times t_{LM}, ranging from 20 μs to 1 s. The number of scans for each experiment was 128, which corresponded to repeating the whole phase cycle eight times. The delay t_{DQ} was 2 μs.

3.3 | Data processing

For each z-spectrum, we integrated the water peak from −400 Hz to 400 Hz.

For each DQF spectrum, we integrated the 1D spectrum from −100 Hz to 200 Hz and from −25 kHz to 20 kHz. We assigned the first integral to water and the difference between two integrals to lipids. All the curves were normalized by the maximum of each curve. The non-linear least squares algorithm was used to fit the DQF data to Equation 2. The relaxation term R_{1w} was constrained as the measured value, and R_{1l} was constrained within the range from 0 to 20/s, since their values did not affect the fitting significantly. In principle, the sum of p_l and p_w should be 1 for an ideal two-site exchange system. The observed lipid signal, however, contains the signal from DMPC, which influences the results. Furthermore, the initial signal normalization can deviate from the ideal behavior due to pulse sequence imperfections or relaxation effects during delays. Therefore, we fitted the DQF spectra without constraining $p_l + p_w = 1$. The fitting parameters are shown in Table 2. We also performed the fitting with the constraint for comparison (Figure S7 and Table S1). The trends in the two types of analyses are very similar to each other. The smaller the fraction of the exchangeable species, the smaller the p_w values obtained, but the extracted exchange rates typically stay the same.

All the data processing and curve fittings were performed in MATLAB R2014b (MathWorks, Natick, MA, USA). The functions *lsqcurvefit* and *nlparci* were used in the curve fitting.

4 | RESULTS AND DISCUSSION

The results from the DQF-MT experiments are presented in Figure 3. For each sample, the water (blue circles) and lipid signals (orange triangles) are plotted against t_{LM}, together with the curves fitted to Equation 2. All the liposome samples displayed buildups of the water signals. Such a

TABLE 2 MT rates *k* and other parameters for five liposome samples obtained from DQF curve fitting

Number	Sample	R_{1w} (1/s) (fixed)	R_{1l} (1/s) (constrained)	*k* (1/s) (with confidence interval)	p_w	p_l
1	DMPC	0.46	1.52 (1.43, 1.60)	484 (−8, 977)	0.06	1
2	DMPC + sphingomyelin	0.48	1.58 (1.40, 1.76)	269.40 (−191, 730)	0.06	1
3	DMPC + cerebrosides	0.52	1.48 (1.09, 1.87)	2.89 (2.10, 3.68)	0.69	0.57
4	DMPC + cholesterol	0.41	1.72 (0.23, 3.20)	1.67 (−1.31, 4.66)	0.33	1
5	DMPC + protein	0.43	1.35 (−1.75, 4.45)	0.78 (−2.19, 3.76)	0.63	0.62

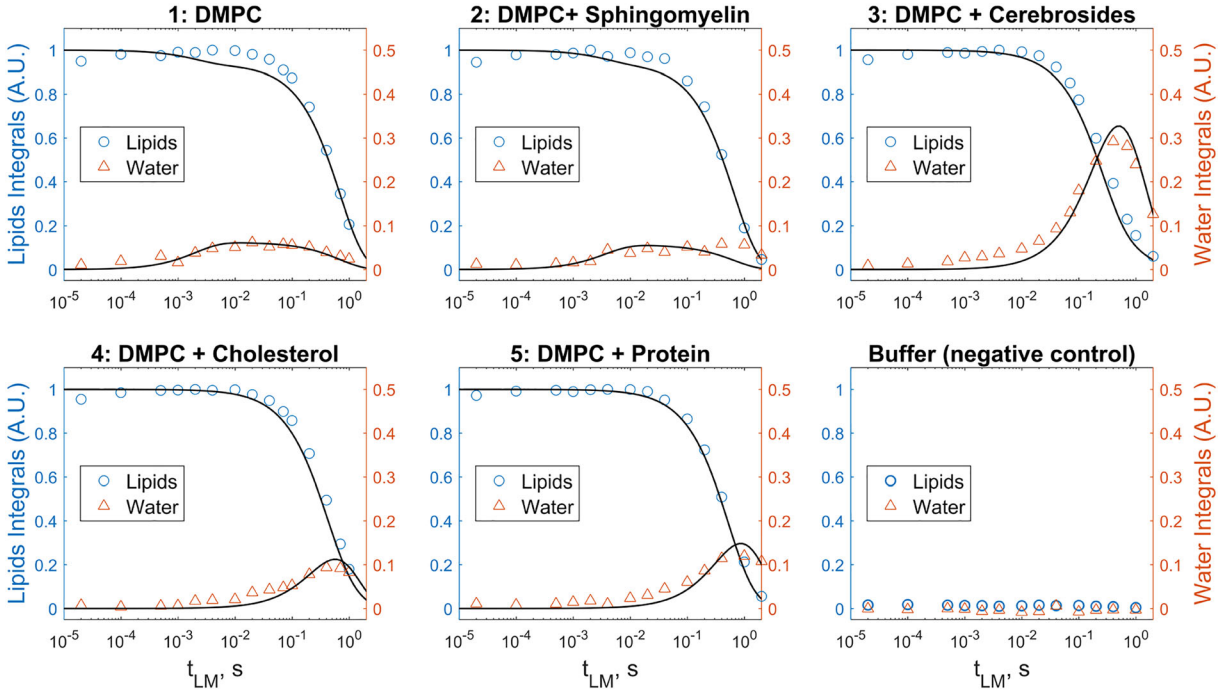

FIGURE 3 DQF-MT integrals for water and lipids shown in separate panels for each sample as a function of t_{LM}. The control experiment is shown in the bottom right panel and represents the negative control for this set of experiments. Data were fitted using equation 1 (solid lines) with the parameters given in Table 2

buildup of the water signal does not exist in a pure buffer solution without any liposomes (control), as shown at the bottom rightmost panel of Figure 3. The sample containing cerebrosides manifested the highest buildup of the water signal. The samples containing protein and cholesterol have the next-highest buildup, and the remaining two samples displayed lower maximum heights of the buildups of the water signals.

The fitted parameters for the DQF data to the model outlined in Section 2 are summarized in Table 2. The low p_w value of the sample containing DMPC corresponded to the fact that the DMPC had no exchangeable proton in its molecular structure. Comparing the samples with cerebrosides and protein, the fitted parameters suggest that their p_w values might be similar, and the MT effects differ due to the exchange rate. The reason why the MT effect is smaller in the sample with cholesterol than in the samples containing cerebrosides and protein might be related to its smaller p_w, ie reduced water access. For the sample containing sphingomyelin, note that likewise the p_w values are relatively low, indicating that water access is much lower than the one to the sugar entities of cerebrosides.

Proton exchange between lipids and free water are influenced by several factors, such as the number of exchangeable groups in lipids, the pH of the sample relative to pertinent pK_a values, and the accessibility of the exchangeable groups to free water. In DMPC, the phosphate group is deprotonated at the pH of the buffer solution used in this work and was expected to have reduced MT effects as observed in experimental data. Sphingomyelin contains one hydroxyl and one amide group, which may be responsible for its MT effect. Cholesterol has only one hydroxyl group but produces a stronger MT effect than sphingomyelin, which is likely due to its lower molecular weight and thus greater number of moles per weight present, since liposome samples were prepared at a constant 10% weight incorporation. Finally, cerebrosides have four hydroxyl groups residing on the hydrophilic head, corresponding to its strongest MT effect.

Proteins have several exchangeable protons present at the backbone and side chain residues. The fitted results shown in Table 2 suggest that the accessibility to free water is similar between protein and cerebroside liposome samples, which is intuitive. The lower exchange rate for protein is surprising nonetheless, resulting in a lower amount of MT relative to cerebroside samples. Figure S7 shows *z*-spectra of all these samples, roughly indicating the relative trends observed here. It is more difficult to extract similar data from *z*-spectra since one cannot cleanly separate the pools. The DQF spectrum provides the opportunity to select the lipid component specifically at the start of each exchange period.

5 | CONCLUSION

In this work, exchange parameters have been determined in samples mimicking myelin composition. The emphasis was on determining the relative contributions to exchange and MT of cerebrosides, sphingomyelin, cholesterol, and protein in DMPC bilayers. A DQF-MT experiment was used to determine exchange rates and relative (accessible) pool sizes. It was found that cerebrosides produced the strongest exchange effects, and it was

surprising that those for proteins were significantly weaker. Furthermore, sphingomyelin and cholesterol showed only minimal transfer, despite having exchangeable groups. These results could help deciphering MT contrast mechanisms in white matter.

ACKNOWLEDGEMENTS

This work was supported in part by the National Institutes of Health (R01EB016045 to A.J.; R01AI108889 to N.J.T.), and in part by the US National Science Foundation (NSF CHE 1710046 to A.J.).

ORCID

Weiqi Yang https://orcid.org/0000-0003-2877-3825
Alexej Jerschow https://orcid.org/0000-0003-1521-9219

REFERENCES

1. Liu Z, Pardini M, Yaldizli O, et al. Magnetization transfer ratio measures in normal-appearing white matter show periventricular gradient abnormalities in multiple sclerosis. *Brain*. 2015;138(Pt 5):1239-1246.
2. Harrison NA, Cooper E, Dowell NG, et al. Quantitative magnetization transfer imaging as a biomarker for effects of systemic inflammation on the brain. *Biol Psychiatry*. 2015;78(1):49-57.
3. Janve VA, Zu Z, Yao SY, et al. The radial diffusivity and magnetization transfer pool size ratio are sensitive markers for demyelination in a rat model of type III multiple sclerosis (MS) lesions. *Neuroimage*. 2013;74:298-305.
4. Schmierer K, Scaravilli F, Altmann DR, Barker GJ, Miller DH. Magnetization transfer ratio and myelin in postmortem multiple sclerosis brain. *Ann Neurol*. 2004;56(3):407-415.
5. Jones CK, Huang A, Xu J, et al. Nuclear Overhauser enhancement (NOE) imaging in the human brain at 7T. *Neuroimage*. 2013;77:114-124.
6. Jones CK, Polders D, Hua J, et al. In vivo three-dimensional whole-brain pulsed steady-state chemical exchange saturation transfer at 7 T. *Magn Reson Med*. 2012;67(6):1579-1589.
7. Ling W, Regatte RR, Navon G, Jerschow A. Assessment of glycosaminoglycan concentration in vivo by chemical exchange-dependent saturation transfer (gagCEST). *Proc Natl Acad Sci U S a*. 2008;105(7):2266-2270.
8. Gass A, Barker GJ, Kidd D, et al. Correlation of magnetization transfer ratio with clinical disability in multiple sclerosis. *Ann Neurol*. 1994;36(1):62-67.
9. Vavasour IM, Laule C, Li DK, Traboulsee AL, MacKay AL. Is the magnetization transfer ratio a marker for myelin in multiple sclerosis? *J Magn Reson Imaging*. 2011;33(3):713-718.
10. Aggarwal S, Yurlova L, Simons M. Central nervous system myelin: structure, synthesis and assembly. *Trends Cell Biol*. 2011;21(10):585-593.
11. Wilhelm MJ, Ong HH, Wehrli SL, et al. Direct magnetic resonance detection of myelin and prospects for quantitative imaging of myelin density. *Proc Natl Acad Sci U S a*. 2012;109(24):9605-9610.
12. Fralix TA, Ceckler TL, Wolff SD, Simon SA, Balaban RS. Lipid bilayer and water proton magnetization transfer: effect of cholesterol. *Magn Reson Med*. 1991;18(1):214-223.
13. Kucharczyk W, Macdonald PM, Stanisz GJ, Henkelman RM. Relaxivity and magnetization transfer of white matter lipids at MR imaging: importance of cerebrosides and pH. *Radiology*. 1994;192(2):521-529.
14. Malyarenko DI, Zimmermann EM, Adler J, Swanson SD. Magnetization transfer in lamellar liquid crystals. *Magn Reson Med*. 2014;72(5):1427-1434.
15. Lee JS, Regatte RR, Jerschow A. Magnetization transfer in a partly deuterated lyotropic liquid crystal by single- and dual-frequency RF irradiations. *J Magn Reson*. 2017;281:141-150.
16. van Zijl PC, Zhou J, Mori N, Payen JF, Wilson D, Mori S. Mechanism of magnetization transfer during on-resonance water saturation. A new approach to detect mobile proteins, peptides, and lipids. *Magn Reson Med*. 2003;49(3):440-449.
17. Eliav U, Navon G. Multiple quantum filtered NMR studies of the interaction between collagen and water in the tendon. *J Am Chem Soc*. 2002;124(12):3125-3132.
18. Zaiss M, Bachert P. Chemical exchange saturation transfer (CEST) and MR Z-spectroscopy *in vivo*: a review of theoretical approaches and methods. *Phys Med Biol*. 2013;58(22):R221-R269.
19. Ge Y, Grossman RI, Babb JS, Rabin ML, Mannon LJ, Kolson DL. Age-related total gray matter and white matter changes in normal adult brain. Part II: quantitative magnetization transfer ratio histogram analysis. *Am J Neuroradiol*. 2002;23(8):1334-1341.
20. Morrison C, Henkelman RM. A model for magnetization transfer in tissues. *Magn Reson Med*. 1995;33(4):475-482.
21. Swanson SD, Malyarenko DI, Fabiilli ML, Welsh RC, Nielsen JF, Srinivasan A. Molecular, dynamic, and structural origin of inhomogeneous magnetization transfer in lipid membranes. *Magn Reson Med*. 2017;77(3):1318-1328.
22. UniProt. https://www.uniprot.org/uniprot/P23895.
23. Xu X, Yadav NN, Zeng H, et al. Magnetization transfer contrast-suppressed imaging of amide proton transfer and relayed nuclear Overhauser enhancement chemical exchange saturation transfer effects in the human brain at 7T. *Magn Reson Med*. 2016;75(1):88-96.
24. Lee JS, Parasoglou P, Xia D, Jerschow A, Regatte RR. Uniform magnetization transfer in chemical exchange saturation transfer magnetic resonance imaging. *Sci Rep*. 2013;3:1707.
25. van Ziji PCM, Yadav NN. Chemical exchange saturation transfer (CEST): what is in a name and what isn't? *Magn Reson Med*. 2011;65(4):927-948.

26. Zaiss M, Schmitt B, Bachert P. Quantitative separation of CEST effect from magnetization transfer and spillover effects by Lorentzian-line-fit analysis of z-spectra. *J Magn Reson*. 2011;211(2):149-155.

27. Edzes HT, Samson RS. The measurement of cross-relaxation effects in the proton NMR spin-lattice of water in biological systems: hydrated collagen and muscle. *J Magn Reson*. 1978;31:207-229.

28. Edzes HT, Samulski ET. Cross relaxation and spin diffusion in the proton NMR of hydrated collagen. *Nature*. 1977;265(5594):521-523.

29. Gayen A, Banigan JR, Traaseth NJ. Ligand-induced conformational changes of the multidrug resistance transporter EmrE probed by oriented solid-state NMR spectroscopy. *Angew Chem Int Ed Engl*. 2013;52(39):10321-10324.

30. Gayen A, Leninger M, Traaseth NJ. Protonation of a glutamate residue modulates the dynamics of the drug transporter EmrE. *Nat Chem Biol*. 2016;12(3):141-145.

SUPPORTING INFORMATION

Additional supporting information may be found online in the Supporting Information section at the end of the article.

How to cite this article: Yang W, Lee J-S, Leninger M, Windschuh J, Traaseth NJ, Jerschow A. Magnetization transfer in liposome and proteoliposome samples that mimic the protein and lipid composition of myelin. *NMR in Biomedicine*. 2019;32:e4097. https://doi.org/10.1002/nbm.4097